ADVANCED FUNCTIONAL MATERIALS
www.afm-journal.de

Materials Views
www.MaterialsViews.com

Tunable Decoration of Reduced Graphene Oxide with Au Nanoparticles for the Oxygen Reduction Reaction

Sung-Soo Kim, Yang-Rae Kim, Taek Dong Chung, and Byeong-Hyeok Sohn**

Reduced graphene oxide (rGO) films are decorated with non-overlapping Au nanoparticles using diblock copolymer micelles that provide controllability over the number density as well as the diameter of the nanoparticles. This synthetic process produces a pure Au surface without extra layers. Furthermore, the rGO film enables the transferability of the Au nanoparticles without deterioration of their arrays. Thus, the controllability of the Au nanoparticles and their transferability with rGO films allow the effective modification of electrochemical electrodes. With a glassy carbon electrode modified with an rGO film with Au nanoparticles, high electrochemical activity is observed in the oxygen reduction reaction (ORR). Furthermore, it is possible to identify a size-dependent ORR mechanism, showing that Au nanoparticles with an average diameter of 8.6 nm exhibit a 4-electron direct reduction of O_2 to H_2O.

1. Introduction

Graphene is a flat monolayer of sp^2 carbon atoms in a two-dimensional honeycomb lattice. It has attracted much attention as a new carbon material because of its optical transparency,[1] superior thermal conductivity,[2] high elasticity,[3] and unique physical phenomena, such as ballistic electron transport.[4] In particular, electronic and electrochemical applications of graphene have been widely studied due to its large specific surface area (2630 m^2 g^{-1}),[5] high electron mobility,[6] and rapid charge transfer[7] compared to graphite and carbon nanotubes. Nevertheless, the mechanical exfoliation method that was initially introduced to obtain graphene can hardly produce graphene with a large area on a substrate. Recently, intensive studies have been performed for the mass production of graphene through chemical vapor deposition or chemical exfoliation of graphite. For example, the Hummers method[8,9] has been used to obtain dispersions of chemically exfoliated graphene oxide (GO) or reduced graphene oxide (rGO) in large quantity, allowing a variety of studies on graphene-based applications, including electrochemical capacitors,[10] biosensing,[11] infrared light detection,[12] and electrocatalysts.[13]

Because graphene has a two-dimensional and conductive structure that can effectively support nanoparticles, many experiments have been carried out to grow or attach highly catalytic nanoparticles of metals or metal oxides such as Pt,[14] Au,[15] Ag,[16] and TiO_2,[17] on graphene sheets for various purposes, including for the enhanced electrocatalytic activity, sensing, and actuating performance of graphene. For example, Dai et al.[18] recently reported the improved catalytic activity of a hybrid material consisting of rGO and Co_3O_4 nanoparticles, compared to that of rGO alone or Co_3O_4 nanoparticles themselves. They ascribed the improved electrocatalytic activity to the synergetic chemical coupling between the rGO and the nanoparticles.

Controlling the size and amount of nanoparticles attached to graphene is of great importance for practical applications, as the electrochemical properties are significantly dependent on these factors.[19] However, current techniques for the attachment of nanoparticles onto graphene do not show sufficient controllability. The majority of the methods to attach, anchor, or grow nanoparticles onto graphene have employed an in situ synthesis of nanoparticles from the precursors at the surface of the GO or rGO.[14–17] Despite the simplistic synthesis of graphene-nanoparticle hybrid materials, the nanoparticles on GO or rGO sheets from the in situ synthesis are generally of an irregular size, shape, and may be agglomerated.

As an alternative method, nanoparticles were synthesized ex situ and then mixed with a GO dispersion to be adsorbed onto the surface of graphene.[20,21] However, the physisorption of nanoparticles onto graphene was not adequate to control the amount of nanoparticles on the graphene, although the size and shape of the ex situ synthesized nanoparticles were regular. Furthermore, stabilizers such as surfactants or polymers on the surface of ex situ synthesized nanoparticles could hinder the catalytic interaction.[22]

Particularly for electrochemical applications, graphene attached with nanoparticles, whether they were synthesized in situ or ex situ, should be coated on carbon electrodes, which presents the challenge of avoiding agglomeration of the graphenes attached with nanoparticles. To take full advantage of the unique characteristics of graphene, such as flexibility, transparency, and transferability,[23] it is necessary to produce aggregation-free nanoparticles on a continuous thin film of graphene. Numerous methods including layer-by-layer assembly, printing-based transfer of nanoparticles, transfer of nanoparticles assembled at an interface, electrodeposition, and sputtering are available to produce nanoparticles on a continuous

S.-S. Kim, Dr. Y.-R. Kim, Prof. T. D. Chung, Prof. B.-H. Sohn
Department of Chemistry
Seoul National University
Seoul 151–747, Korea
E-mail: tdchung@snu.ac.kr; bhsohn@snu.ac.kr

DOI: 10.1002/adfm.201303968

substrate.[24] However, few of these methods can satisfy the requirement of synthesizing aggregation-free nanoparticles with tunable size and number density on a continuous, large-area graphene sheet.

The diblock copolymer approach has been used to synthesize arrayed nanoparticles on large-area substrates and is a potential candidate to decorate nanoparticles on graphene to meet the criteria of synthesizing aggregation-free nanoparticles with controllability.[25] Diblock copolymers, consisting of two chemically distinct homopolymers linked by a covalent bond, spontaneously assemble into a variety of periodic nanostructures. Their size and morphology can be easily adjusted by varying the molecular weight, the relative volume fraction, and the interaction parameter of the copolymer. Ordered nanostructures of diblock copolymers have been utilized as templates or lift-off masks to fabricate arrays of diverse nanoparticles on various substrates.[25]

To apply the nanostructures of copolymers to graphene, however, the surface of graphene should be chemically modified[26,27] or covered with an additional layer[28–31] to induce perpendicularly oriented nanostructures, which are necessary for the application of diblock copolymers to templates and masks. To avoid additional treatment of the graphene surface, an approach involving nanoscale micelles of diblock copolymers may be a plausible answer for the tunable synthesis of nanoparticles on graphene.

When diblock copolymers are dissolved in a selective solvent for one of the blocks, spherical micelles with a soluble corona and an insoluble core can be obtained. Because we can load nanoparticle precursors into the cores of copolymer micelles and spin-coat a single layer of micelles without overlapping, we can effectively synthesize nanoparticles on a variety of substrates by post-treatment of the micellar layer.[32–35] The diameter and inter-distance of the micelles, which can be adjusted by the molecular weight of the copolymer, govern the size and spacing of the nanoparticles that are synthesized from the micelles.[35–38] Thus, graphene can be decorated with tunable nanoparticles by coating diblock copolymer micelles directly on the surface of graphene.

In this study, we first decorated rGO films with arrays of Au nanoparticles using diblock copolymer micelles. The rGO film with Au nanoparticles was transferable without deterioration of the Au nanoparticles array. Next, we modified glassy carbon electrodes by transferring the rGO decorated with Au nanoparticles, which showed high electrocatalytic performance in a redox reaction. In addition, we applied rGO films with Au nanoparticles to the oxygen reduction reaction (ORR), which is an important electrochemical reaction for a variety of energy conversion devices, including fuel cells. Furthermore, we were able to differentiate the ORR mechanisms between Au nanoparticles having different diameters, which were effectively controlled by the micellar dimensions.

2. Results and Discussion

We prepared an aqueous dispersion of GO from graphite powders by the modified Hummers method[8,9] and spin-coated GO onto a Si substrate having a 300-nm-thick oxide layer (denoted as a SiO_2/Si substrate hereafter). The spin-coated GO shows overlapped flakes having a thickness of ≈1 nm (Figure S1a, Supporting Information). Successive spin-coating provided continuous, two-dimensional GO films with a large area. The thickness was controllable by adjusting the concentration of the GO dispersion, the spinning speed, and the number of repeats of spin-coating.[39] The spin-coated GO was then reduced to rGO using hydrazine as a reducing agent. The rGO film showed a uniform surface with a thickness of ≈2.3 nm (Figure S1b, Supporting Information). On such an rGO film, we synthesized arrays of Au nanoparticles which are known to exhibit distinctive catalytic activity compared to their bulk counterpart.[40]

We first coated the surface of the rGO films with a single layer of PS-P4VP (109 k–27 k) micelles with $HAuCl_4$, the precursor of Au nanoparticles, in the P4VP cores. The AFM image in **Figure 1**a shows an array of spherical micelles without overlapping, implying a single layer of copolymer micelles. Then, we removed the copolymers by heating, which resulted in the generation of Au nanoparticles in the core regions of the micelles as shown in Figure 1b. The spacing (≈111 nm) and number density (≈7.60×10^9 cm^{-2}) of the Au nanoparticles measured by fast Fourier transformation (FFT) analysis are similar to those of the original copolymer micelles (≈118 nm and ≈7.62×10^9 cm^{-2}), implying successful fabrication of an array of non-overlapped Au nanoparticles directly decorated on rGO with preservation of the order of the copolymer micelles. It is worthwhile to note that Au nanoparticles with well-defined spacing and without agglomeration could not be easily synthesized on rGO by either in situ or ex situ methods.

In the XPS analysis of the nanoparticles (Figure S2a, Supporting Information), no peaks associated to oxides were observed, indicating pure Au nanoparticles. We note that the free energy of formation of Au oxides is positive and becomes more positive at elevated temperatures because of the positive enthalpy of formation of Au oxides and the negative entropic change for the oxidation reaction of metal elements. Thus, the formation of Au oxides at elevated temperatures is not favored. Because rGO films can be delaminated from SiO_2/Si substrates by exposing them to a solution of NaOH,[41] we were able to transfer them onto a copper grid for TEM analysis. In Figure 1c, we can clearly see non-overlapped Au nanoparticles with more or less regular spacing on the rGO film whose edge is visible at the left side of the image. The Au nanoparticles have an average diameter of 11.0 m (±5.5 nm) (histogram in Figure 1d) and a face-centered cubic crystalline structure (HR-TEM in Figure 1c and selected area electron diffraction pattern in Figure S2b, Supporting Information). More importantly, this TEM image confirms that the array of Au nanoparticles on the rGO was well maintained during the transfer process, suggesting that it is possible to transfer Au nanoparticles on rGO to any substrate, including a hydrophobic glassy carbon electrode or a flexible polymer film (Figure 1c). Moreover, no additional layer was observed on the surface of the Au nanoparticles in the HR-TEM image (Figure 1c), indicating a pure Au surface, which is particularly suitable for catalytic applications.[42] In addition, we obtained the height profiles of Au nanoparticles by AFM (Figure S3, Supporting Information). The clean and smooth Au surfaces were observed without any patches and residues, indicating the absence of any extra layers on the Au surfaces.

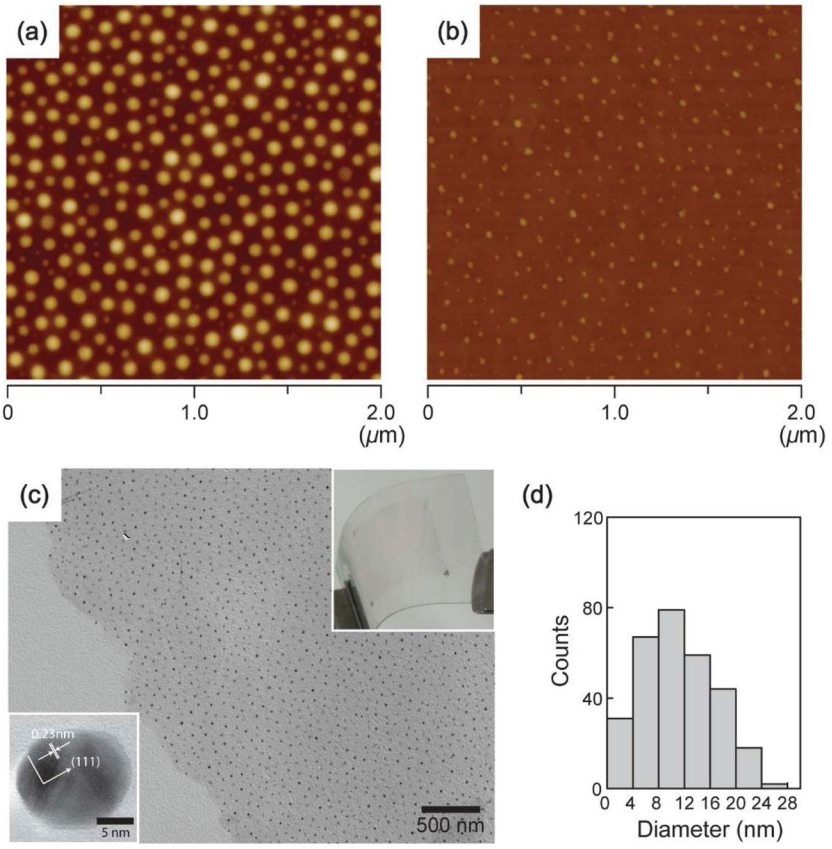

Figure 1. a) AFM image of PS-P4VP (109 k–27 k) micelles on rGO; b) AFM image of Au nanoparticles synthesized from the micelles; c) TEM image of Au nanoparticles on rGO; d) the diameter distribution of the Au nanoparticles measured from the TEM image. The insets in (c) are the HR-TEM image of an individual Au nanoparticle and the photo of a transferred rGO film with Au nanoparticles (the gray square) on a flexible polymer film.

One of the merits of the diblock copolymer micellar approach to synthesize nanoparticles is the controllability of the number density and the size of the nanoparticles by adjusting the molecular weights of the copolymer.[35–38] To demonstrate this controllability, we employed a lower molecular weight copolymer PS-P4VP (51 k–18 k) than previously utilized PS-P4VP (109 k–27 k). We repeated the same procedure as before to synthesize Au nanoparticles on rGO films. Because both core and corona are smaller than before, and they effectively govern the diameter and the spacing of the synthesized nanoparticles, respectively, the average diameter of the Au nanoparticles was reduced to 8.6 nm (±4.0 nm) (**Figure 2**d), and the spacing also decreased to ~53 nm, which results in a 4.8-fold increase in the number density (≈3.62×10^{10} cm^{-2}). The more crowded nanoparticles are visible in the AFM (Figure 2b) and TEM images (Figure 2c). However, we still have a single layer of Au nanoparticles without agglomeration or overlapping. Thus, we were able to efficiently produce rGO films decorated with smaller Au nanoparticles in a higher number density.

Another merit of the diblock copolymer micellar approach is the synthesis of diverse nanoparticles by changing the precursors loaded into the cores of the copolymer.[32,36,38] Thus, we were also able to fabricate rGO decorated with a single layer of iron oxide nanoparticles without agglomeration by altering the precursor from $HAuCl_4$ to $FeCl_3$, which were loaded in the P4VP cores of PS-P4VP (51 k–18 k) micelles (Figure S4, Supporting Information).

As we demonstrated, the diblock copolymer micellar approach allows the decoration of Au nanoparticles on rGO films with controllable diameter and number density. Furthermore, when TEM samples were prepared, the array of Au nanoparticles on rGO films was not affected during the transfer, indicating that we can modify an electrochemical electrode by transferring rGO films decorated with Au nanoparticles as they were made. Thus, we applied the rGO films with Au nanoparticles to electrochemical reactions, including ORR.

Before characterizing the ORR performance, we investigated the general electrocatalytic features of rGO decorated with Au nanoparticles by studying the redox reaction of $Fe(CN)_6^{3-/4-}$ with electrochemical impedance spectroscopy (EIS) and cyclic voltammetry (CV). We first modified a glassy carbon electrode (GCE) by transferring the rGO films with Au nanoparticles directly onto a GCE, as demonstrated with a flexible polymer film as well as a TEM sample (Figures 1c, 2c). Hereafter, we denote Au nanoparticles synthesized from PS-P4VP (109 k–27 k) and PS-P4VP (51 k–18 k) as Au(109 k–27 k) and Au(51 k–18 k), respectively. We again note that Au(51 k–18 k) has a smaller diameter with a higher number density than Au(109 k–27 k).

In the Nyquist plot of **Figure 3**a, the diameter of a semicircle corresponds to the charge transfer resistance (R_{ct} in the equivalent circuit) at the interface between electrodes and electrolytes during the electrochemical reaction.[43] The rGO alone exhibits a semicircle with an electrical resistance of ≈191 Ω, whereas both rGO films decorated with Au nanoparticles do not show semicircles as the GCE itself, implying very low resistances. We observed similar results when ITO electrodes were employed instead of a GCE (Figure S5, Supporting Information). Because rGO films consist of flakes, there could be a discontinuity in the films due to defects of oxygen-containing functional groups such as hydroxyls and epoxides even after the reduction process of GO.[44] Such discontinuity could cause a high resistance to charge transfer. However, the decoration of Au nanoparticles on rGO films effectively revealed the decreased resistance, presumably by providing electrical connectivity between rGO flakes. The low resistances of rGO with Au nanoparticles are advantageous for electrocatalytic applications.

Both rGO films decorated with Au nanoparticles exhibited higher peak currents and smaller peak potential differences than rGO itself, as shown by the CV data of the redox reaction of $Fe(CN)_6^{3-/4-}$ (Figure 3b), implying the enhancement of the electrocatalytic activities of rGO films by Au nanoparticles.[45]

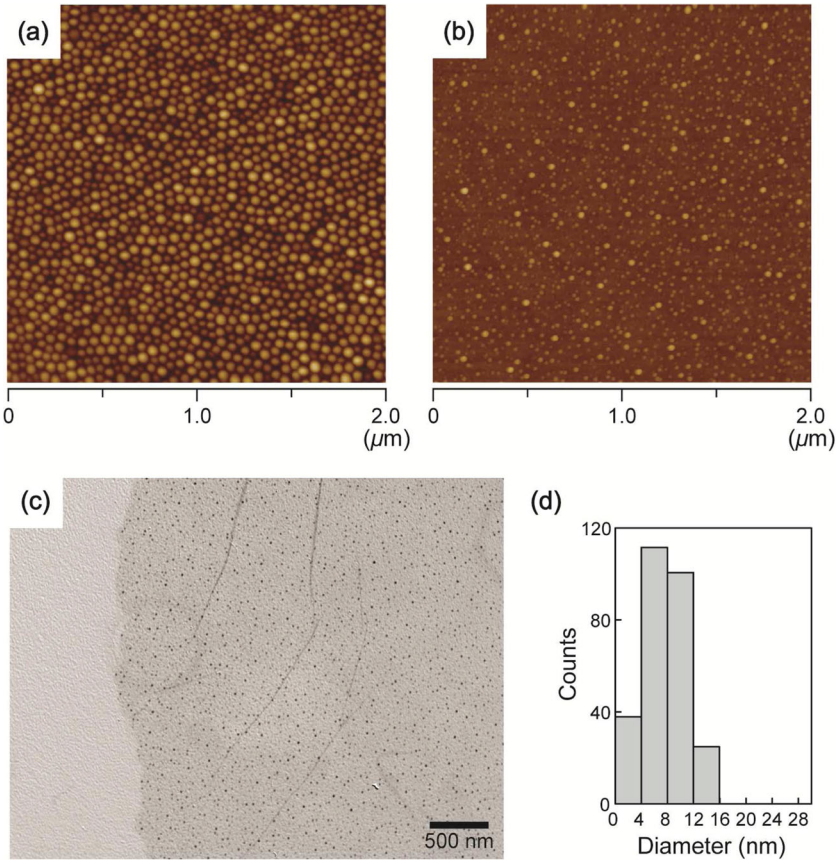

Figure 2. a) AFM image of PS-P4VP (51 k–18 k) micelles on rGO; b) AFM image of the Au nanoparticles synthesized from the micelles; c) TEM image of the Au nanoparticles on rGO; d) diameter distribution of the Au nanoparticles measured from the TEM image.

We also found that the peak current was linearly proportional to the square root of the scan rate, indicating that the electrochemical reaction on the rGO film decorated with Au nanoparticles is diffusion-controlled, that is, a kinetically fast process (Figure S6, Supporting Information).[46] We note that Au(51 k–18 k) shows superior activity to Au(109 k–27 k), which can be attributed to the larger electrochemical surface of Au(51 k–18 k). Thus, we expect that decorating rGO films with Au nanoparticles will be beneficial for electrocatalytic applications, including the oxygen reduction reaction (ORR).

We further characterized the ORR performance of rGO films decorated with Au nanoparticles under basic conditions (an oxygen-saturated KOH solution), which is relevant to practical applications such as fuel cells.[47] Because the ORR is an irreversible reaction, a single peak current was detected at –0.34 V for rGO films with Au nanoparticles, but not for rGO alone (**Figure 4**). A high peak current implies not only effective transfer of a large number of electrons to oxygen molecules but also reduction of more oxygen molecules in the time unit with the same number of electrons per oxygen molecule. Thus, decorating rGO with Au nanoparticles increased the ORR activity of rGO. We verified that the peaks were primarily associated with the ORR by observing that the magnitude of the peak current depended on the oxygen content in the solution (Figure S7, Supporting Information). In Figure 4, Au(51 k–18 k) shows a higher peak current (265 μA) than Au(109 k–27 k) (194 μA), indicating that more oxygen molecules can interact with smaller and denser Au nanoparticles available in the same area. Therefore, we can attain high electrochemical performance with rGO films decorated with Au nanoparticles. We note that similar results were also observed under acidic conditions (an oxygen-saturated H_2SO_4 solution) (Figure S8, Supporting Information).

To determine the effect of the Au nanoparticles themselves (without rGO) on the ORR activity, decorating Au nanoparticles directly on a GCE is required. Without rGO films, however, it is nearly impossible to synthesize well-defined Au nanoparticles on the surface of a GCE at the same level of quality as demonstrated on rGO films. An attempt to synthesize Au nanoparticles directly on a GCE using copolymer micelles was not successful. The transferability enabled by rGO films is necessary to decorate an array of Au nanoparticles on the electrode.

Electrochemical analysis based on a rotating disk electrode (RDE) was also carried out to study the difference in ORR activities between two different Au nanoparticle cases, that is, Au(109 k–27 k) and Au(51 k–18 k). In this system, the Au nanoparticles, which were uniformly distributed on a single graphene sheet, had pure Au surfaces without any extra layers and no additional material such as Nafion was required to stabilize them on the rapidly rotating electrode. Therefore, we can assume that all Au nanoparticles were equally exposed to reactants, for example, oxygen in this case. Furthermore, we were able to conduct a rigorous electrochemical evaluation of the Au nanoparticles on rGO films owing to the unusual transferability of this system to the RDE. The rGO with Au nanoparticles transferred onto the RDE was confirmed to be very stable; no decrease of the electrochemical activity after several repeats of the measurement was observed.

In most cases, ORR electrocatalysts are evaluated on an RDE after being mixed with commercialized carbon and Nafion as a stabilizer. This methodology can deteriorate the electrocatalysts and deter the mass transfer by the aggregation and/or agglomeration of carbon and nanoparticles. Furthermore, Nafion is temperature dependent, which is a critical problem in the development of practical fuel cell systems. In this sense, the proposed system possesses a nearly ideal structure of the triple-phase boundary for electrocatalysis. We used an rGO film, on which all of the nanoparticles were exposed to the solution without any stabilizer. Calcination by heat treatment, as shown in Figure 1c, and the absence of stabilizer ensured that all Au nanoparticles on the rGO were clean enough to maximize their electrocatalytic activity.

In the linear-sweep voltammetry (LSV) curves of **Figure 5**, the currents for both Au nanoparticles increased with an increase in

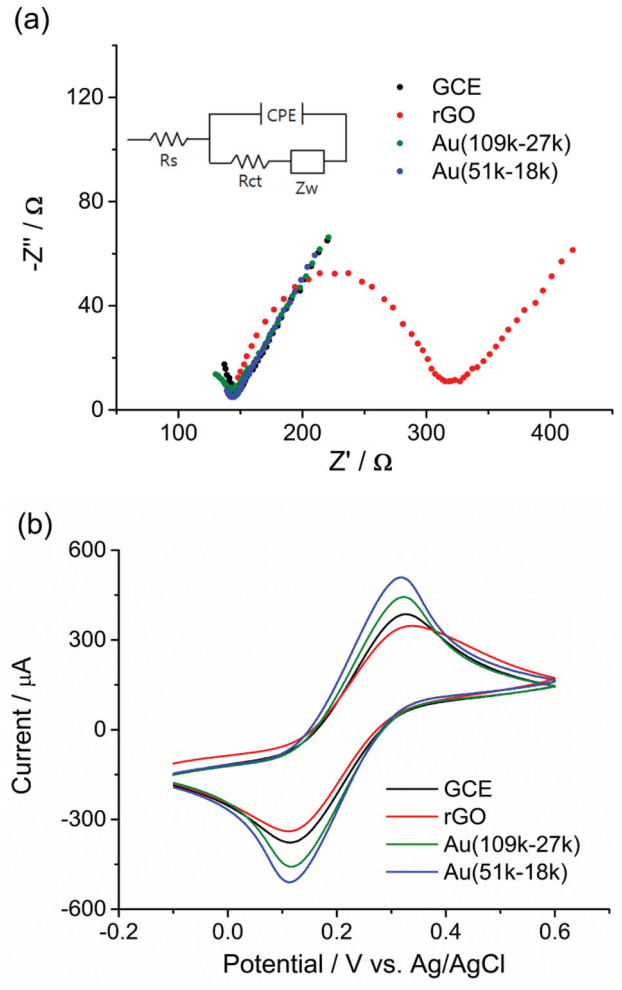

Figure 3. a) Nyquist plots and b) cyclic voltammograms of $Fe(CN)_6^{3-/4-}$. The inset in (a) is an equivalent circuit to fit EIS data, where R_s, R_{ct}, Z_w, and CPE are the solution resistance, the charge transfer resistance, the Warburg impedance, and the constant phase element, respectively. The scan rate was 100 mV s^{-1}.

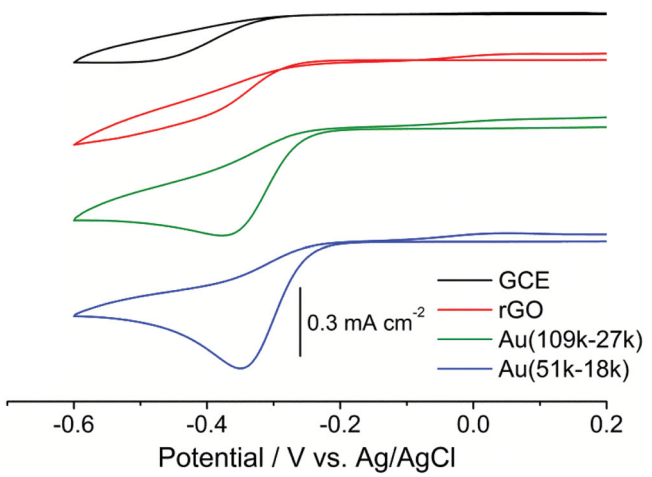

Figure 4. Cyclic voltammograms for ORR with rGO films decorated with Au nanoparticles in oxygen-saturated 0.1 M KOH solutions. The scan rate was 50 mV s^{-1}.

the rotating rate because more reactants can reach the electrode at faster rotations. From the LSV data from –0.4 V to –0.5 V, we obtained Koutecky-Levich plots, that is, (current density)$^{-1}$ versus (rotating rate)$^{-1}$, which are shown in Figure 5c. For clarity, only the plots at –0.45 V and –0.5 V are displayed. We can extract the number of electrons involved in the ORR from the slope of each plot. In the case of Au(109 k–27 k), the slopes were in the range of 1.7–2.3, indicating a dominant 2-electron process, that is, reduction of O_2 to H_2O_2.[48] In contrast, we obtained slopes of 3.7–4.0 for Au(51 k–18 k), which implies a 4-electron process, *i.e.*, direct reduction of O_2 to H_2O, which is desirable for practical applications.[48] According to previous studies on the ORR with Au nanoparticles, the occurrence of a 2- or 4-electron process is primarily dependent on the size of the Au nanoparticles.[19,49] In addition, denser nanoparticles can have a higher probability to reduce the desorbed H_2O_2 to H_2O in the scheme of desorption, re-adsorption, and reduction.[50,51] Au nanoparticles with a diameter smaller than 10 nm undergo a 4-electron process, which explains our observations: a 4-electron process for Au(51 k–18 k), having an average diameter of 8.6 nm with a higher number density, and a 2-electron process for Au(109 k–27 k), having an average diameter of 11 nm with a lower number density.[19,49] We note that 2- and 4-electron reactions could not occur completely independently because of the size distribution of the Au nanoparticles, as shown in Figures 1d, 2d. We also confirmed the electrochemical stability of the Au nanoparticles; there were no noticeable changes in the current of the ORR with Au nanoparticles at a constant potential of –0.6 V after 2 h (Figure S9, Supporting Information), although this condition is not related to an accelerated stress test protocol. Thus, we demonstrated that the controllability of the size of Au nanoparticles with copolymer micelles and the transferability of nanoparticles with rGO films enabled the fabrication of rGO films decorated with Au nanoparticles, which are suitable for practical ORR applications and exhibited a 4-electron reduction process.

3. Conclusions

The approach with PS-P4VP copolymer micelles allowed the decoration of non-overlapping Au nanoparticles on rGO films with controllable diameter and number density. These factors were effectively controlled by the molecular weights of the PS-P4VP copolymer. The Au nanoparticles have a pure Au surface without extra layers. These rGO films with Au nanoparticles were transferred onto a glassy carbon electrode without deterioration of the array of Au nanoparticles. They showed high electrocatalytic activities in the redox reaction of $Fe(CN)_6^{3-/4-}$ and the ORR. Furthermore, we were able to differentiate the ORR mechanisms of Au(109 k–27 k) and Au(51 k–18 k) by RDE analysis. Au(51 k–18 k) has a smaller diameter and mainly exhibited a 4-electron direct reduction pathway of O_2 to H_2O. Thus, the controllability of the size of the Au nanoparticles with copolymer micelles and their transferability made the proposed system suitable for ORR applications. The electrocatalytic activities were enhanced by the clean surfaces of the

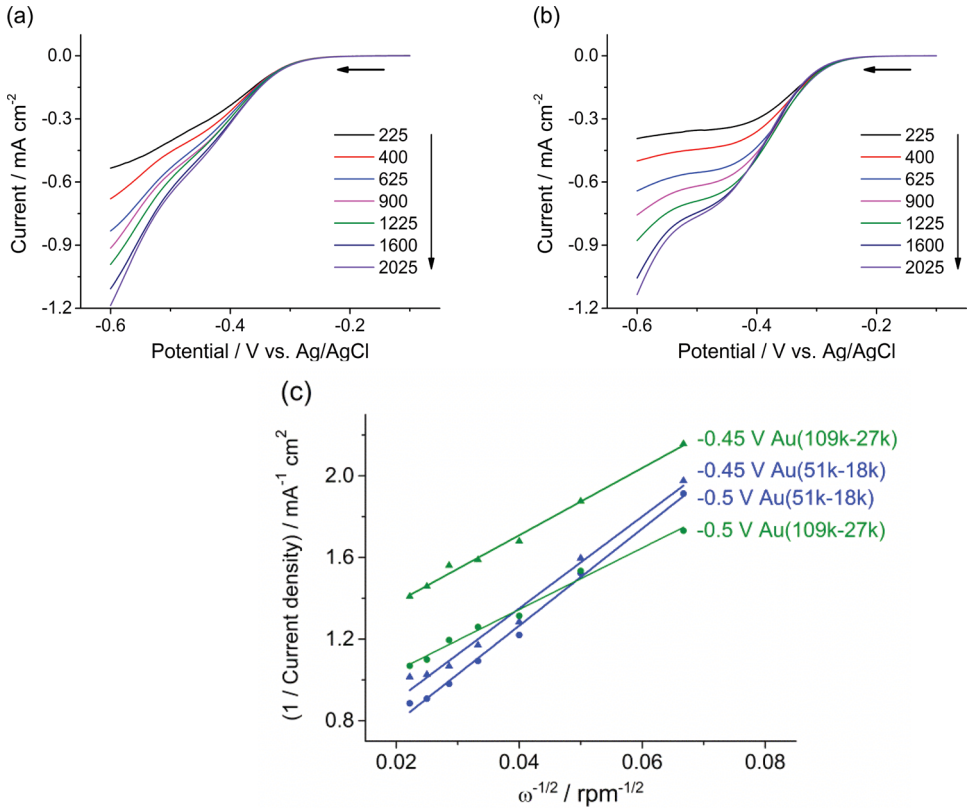

Figure 5. Linear sweep voltammograms for the ORR with rGO films decorated with Au nanoparticles in oxygen-saturated 0.1 M KOH solutions on a) Au(109 k–27 k) and b) Au(51 k–18 k); c) Koutecky-Levich plots. The scan rate was 5 mV s^{-1}. The numbers shown in the voltammograms are the rotating rates in rpm. The arrows indicate the scan direction. The background current in an oxygen-free solution was subtracted.

Au nanoparticles on the rGO, which were prepared by calcination and stabilizer-free processes. It is possible to obtain arrays of various metal or metal oxide nanoparticles on graphene with tunable number density and size simply by changing the precursors and molecular weights of the diblock copolymer micelles. In addition, the facile, large-area synthesis of rGO films decorated with nanoparticles would be an interesting target. The methodology of combining copolymer micelles and rGO films can be extended to prepare various nanoparticles on graphene in a controlled way, which has potential in numerous applications, including biosensors, supercapacitors, and electro- and photo-catalysts.

4. Experimental Section

Diblock Copolymer Micelles Containing Precursors of Nanoparticles: We purchased two diblock copolymers of polystyrene-poly(4-vinyl pyridine): PS-P4VP (109 k–27 k) and PS-P4VP (51 k–18 k) from Polymer Source Inc. The number in the parentheses is the molar mass of each block in g/mol. The polydispersity index of both copolymers is 1.15. PS-P4VP diblock copolymers were dissolved in toluene, a strongly selective solvent for the PS block, with a concentration of 0.5 wt%. The solution was stirred for 24 h at room temperature and for 3 h at 85 °C and then cooled to room temperature. $HAuCl_4$ or $FeCl_3$, precursors of gold and iron oxide nanoparticles, respectively, were added to the micellar solution. The molar ratio of precursors to pyridine units in the P4VP block was fixed at 0.5 for both cases. The solution was stirred for at least 7 days at room temperature.

rGO Films Decorated with Nanoparticles: Graphene oxides (GO) were synthesized by the modified Hummers method as described elsewhere.[8,9] GO powder was added to DI water (0.1 wt%), which was ultrasonicated for 2 h, followed by centrifugation at 3000 rpm for 1 h and removal of the precipitates, resulting in a yellow-brown homogeneous dispersion. A silicon wafer with a thermally grown oxide layer (300 nm in thickness) was cleaned in piranha solution (70/30 v/v concentrated H_2SO_4 and 30% H_2O_2) at 90 °C for 30 min, and thoroughly rinsed with deionized water several times, and then blown dry with nitrogen. On the cleaned substrate, a continuous GO layer was spin-coated five times at 2000 rpm for 30 s and dried in a vacuum oven at 40 °C overnight. Chemical reduction of GO films was carried out by hydrazine vapor. A fully dried GO film on the substrate was placed in a jar containing hydrazine monohydrate (98%, Sigma-Aldrich) and heated at 160 °C for 1 day. On this reduced graphene oxide (rGO) film, a layer of PS-P4VP micelles containing the precursors of nanoparticles in their cores was spin-coated, typically at 2000 rpm for 60 s. To synthesize the nanoparticles along with the removal of the copolymer, the rGO film decorated with the copolymer micelles was heated in air at 400 °C for 30 min.

Transfer of rGO Films with Nanoparticles onto Various Substrates: Poly(methyl methacrylate) (PMMA) (M_n = 51 k, PDI = 1.06) was dissolved in toluene with a concentration of 1 wt% and spin-coated onto an rGO film decorated with arrays of nanoparticles prepared on a silicon wafer having a thermal oxide top. An additional thick PMMA film was drop-cast on top of the spin-coated PMMA. A droplet of NaOH solution (0.1 M) was added to an edge of the substrate, which led to delamination of the rGO film from the substrate. The delaminated film floated off onto deionized water and was transferred to a designated substrate such as a glassy carbon electrode or an ITO-coated glass for electrochemical measurements. The transferred film was dried under ambient conditions

overnight. For the removal of the PMMA supporting layer, the composite film was heated in air at 400 °C for 30 min or immersed in acetone for 1 h.

Electrochemical Measurements: Cyclic voltammograms, Nyquist plots, amperometry curves, and linear sweep voltammograms were obtained with a CHI 660A electrochemical workstation (CH instruments). For electrochemical measurements, glassy carbon plate electrodes (ALS Co.) and ITO-coated glass substrates were used. The geometric surface area was 0.28 cm^2. A glassy carbon disk electrode with a diameter of 5 mm (Pine Research Instrumentation) was employed as a rotating disk electrode (RDE). Glassy carbon and rotating disk electrodes were carefully polished with alumina powder and rinsed with double distilled water to remove alumina residues. A platinum wire was used as a counter electrode and Ag/AgCl as a reference electrode. 0.01 M phosphate buffered saline (PBS) containing 5 mM of $Fe(CN)_6^{3-/4-}$ (1:1) was used for electrochemical characterizations. Nyquist plots were recorded at the equilibrium potential of $Fe(CN)_6^{3-/4-}$ over the frequency range of 0.5 to 1000 Hz. The impedance data were analyzed using Zsimpwin 3.0 software (Echem Software).

Characterization: rGO films, PS-P4VP micelles, and rGO films with nanoparticles were analyzed using a Multimode 8 atomic force microscope (AFM) with a Nanoscope V controller (Bruker) in tapping mode with Al-coated Si cantilevers. For transmission electron microscopy (TEM), rGO films with nanoparticles were floated off from the substrate onto deionized water by delamination with NaOH solution, as described above, and collected on carbon-coated copper TEM grids. TEM was performed on a Hitachi 7600 operating at 100 kV, a JEM-2100 (JEOL) at 200 kV, and a JEM-3010 (JEOL) at 300 kV. X-ray photoelectron spectroscopy (XPS) was performed using a Sigma Probe (ThermoVG) with a monochromatic Al Kα X-ray source operating at 100 W.

Supporting Information

Supporting Information is available from the Wiley Online Library or from the author.

Acknowledgements

S.-S.K. and Y.-R.K. contributed equally to this work. This work was supported by the Global Frontier R&D Programs on the Center for Advanced Soft Electronics (No. 2011–0031635) and the Nano Material Technology Development Program (No. 2011-0030268) through the National Research Foundation of Korea(NRF) funded by the Ministry of Science, ICT and Future Planning, Korea.

Received: November 25, 2013
Revised: December 12, 2013
Published online: February 3, 2014

[1] R. R. Nair, P. Blake, A. N. Grigorenko, K. S. Novoselov, T. J. Booth, T. Stauber, N. M. R. Peres, A. K. Geim, *Science* **2008**, *320*, 1308.
[2] A. A. Baladin, S. Ghosh, W. Bao, I. Calizo, D. Teweldebrhan, F. Miao, C. N. Lau, *Nano Lett.* **2008**, *8*, 902.
[3] C. Lee, X. D. Wei, J. W. Kysar, J. Hone, *Science* **2008**, *321*, 385.
[4] K. S. Novoselov, A. K. Geim, S. V. Morozov, D. Jiang, Y. Zhang, S. V. Dubonos, I. V. Grigorieva, A. A. Firsov, *Science* **2004**, *306*, 666.
[5] S. Stankovich, D. A. Dikin, G. H. B. Dommett, K. M. Kohlhaas, E. J. Zimney, E. A. Stach, R. D. Piner, S. T. Nguyen, R. S. Ruoff, *Nature* **2006**, *442*, 282.
[6] S. V. Morozov, K. S. Novoselov, M. I. Katsnelson, F. Schedin, D. C. Elias, J. A. Jaszczak, A. K. Geim, *Phys. Rev. Lett.* **2008**, *100*, 016602.
[7] W. Li, M. A. Lowe, H. D. Abruña, D. C. Ralph, *ACS Nano* **2011**, *5*, 2264.
[8] W. S. Jr. Hummers, R. E. Offeman, *J. Am. Chem. Soc.* **1958**, *80*, 1339.
[9] N. I. Kovtyukhova, P. J. Ollivier, B. R. Martin, T. E. Mallouk, S. A. Chizhik, E. V. Buzaneva, A. D. Gorchinskiy, *Chem. Mater.* **1998**, *11*, 771.
[10] M. D. Stoller, S. Park, Y. Zhu, J. An, R. S. Ruoff, *Nano Lett.* **2008**, *8*, 3498.
[11] M. Zhou, Y. Zhai, S. Dong, *Anal. Chem.* **2009**, *81*, 5603.
[12] B. Chitara, L. S. Panchakarla, S. B. Krupanidhi, C. N. R. Rao, *Adv. Mater.* **2011**, *23*, 5419.
[13] L. Tang, Y. Wang, Y. Li, H. Feng, J. Lu, J. Li, *Adv. Funct. Mater.* **2009**, *19*, 2782.
[14] B. Seger, P. V. Kamat, *J. Phys. Chem. C* **2009**, *113*, 7990.
[15] R. Muszynski, B. Seger, P. V. Kamat, *J. Phys. Chem. C* **2008**, *112*, 5263.
[16] L. Lu, J. Liu, Y. Hu, Y. Zhang, W. Chen, *Adv. Mater.* **2013**, *25*, 1270.
[17] I. V Lightcap, T. H. Kosel, P. V Kamat, *Nano Lett.* **2010**, *10*, 577.
[18] Y. Liang, Y. Li, H. Wang, J. Zhou, J. Wang, T. Regier, H. Dai, *Nat. Mater.* **2011**, *10*, 780.
[19] W. Chen, S. Chen, *Angew. Chem. Int. Ed.* **2009**, *48*, 4386.
[20] W. Hong, H. Bai, Y. Xu, Z. Yao, Z. Gu, G. Shi, *J. Phys. Chem. C* **2010**, *114*, 1822.
[21] F. Xiao, J. Song, H. Gao, X. Zan, R. Xu, H. Duan, *ACS Nano* **2012**, *6*, 100.
[22] D. Li, C. Wang, D. Tripkovic, S. Sun, N. M. Markovic, V. R. Stamenkovic, *ACS Catal.* **2012**, *2*, 1358.
[23] Y. Zhu, S. Murali, W. Cai, X. Li, J. W. Suk, J. R. Potts, R. S. Ruoff, *Adv. Mater.* **2010**, *22*, 3906.
[24] A. N. Shipway, E. Katz, I. Willner, *ChemPhysChem* **2000**, *1*, 18.
[25] I. W. Hamley, *Nanotechnology* **2003**, *14*, R39.
[26] B. H. Kim, J. Y. Kim, S. Jeong, J. O. Hwang, D. H. Lee, D. O. Shin, S. Choi, S. O. Kim, *ACS Nano* **2010**, *4*, 5464–5470.
[27] J. Y. Kim, B. H. Kim, J. O. Hwang, S.-J. Jeong, D. O. Shin, J. H. Mun, Y. J. Choi, H. M. Jin, S. O. Kim, *Adv. Mater.* **2013**, *25*, 1331.
[28] J. Bai, X. Zhong, S. Jiang, Y. Huang, X. Duan, *Nat. Nanotechnol.* **2010**, *5*, 190.
[29] M. Kim, N. S. Safron, E. Han, M. S. Arnold, P. Gopalan, *Nano Lett.* **2010**, *10*, 1125.
[30] G. Liu, Y. Wu, Y.-M. Lin, D. B. Farmer, J. a Ott, J. Bruley, A. Grill, P. Avouris, D. Pfeiffer, A. a Balandin, C. Dimitrakopoulos, *ACS Nano* **2012**, *6*, 6786.
[31] X. Liang, S. Wi, *ACS Nano* **2012**, *6*, 9700.
[32] B.-H. Sohn, J.-M. Choi, S. I. Yoo, S.-H. Yun, W.-C. Zin, J. C. Jung, M. Kanehara, T. Hirata, T. Teranishi, *J. Am. Chem. Soc.* **2003**, *125*, 6368.
[33] J. P. Spatz, T. Herzog, S. Mößmer, P. Ziemann, M. Möller, *Adv. Mater.* **1999**, *11*, 149.
[34] A. Ethirajan, U. Wiedwald, H.-G. Boyen, B. Kern, L. Han, A. Klimmer, F. Weigl, G. Kästle, P. Ziemann, K. Fauth, J. Cai, R. J. Behm, A. Romanyuk, P. Oelhafen, P. Walther, J. Biskupek, U. Kaiser, *Adv. Mater.* **2007**, *19*, 406.
[35] M. Aizawa, J. M. Buriak, *J. Am. Chem. Soc.* **2005**, *127*, 8932.
[36] S. I. Yoo, J.-H. Kwon, B.-H. Sohn, *J. Mater. Chem.* **2007**, *17*, 2969.
[37] J. P. Spatz, S. Mößmer, C. Hartmann, M. Möller, T. Herzog, M. Krieger, H.-G. Boyen, P. Ziemann, B. Kabius, *Langmuir* **2000**, *16*, 407.
[38] S. Förster, M. Antonietti, *Adv. Mater.* **1998**, *10*, 195.
[39] G. Eda, M. Chhowalla, *Adv. Mater.* **2010**, *22*, 2392.
[40] M. Haruta, N. Yamada, T. Kobayashi, S. Iijima, *J. Catal.* **1989**, *115*, 301.
[41] J. T. Robinson, M. Zalalutdinov, J. W. Baldwin, E. S. Snow, Z. Wei, P. Sheehan, B. H. Houston, *Nano Lett.* **2008**, *8*, 3441.
[42] H. Yin, H. Tang, D. Wang, Y. Gao, Z. Tang, *ACS Nano* **2012**, *6*, 8288.
[43] Y.-R. Kim, S. Bong, Y.-J. Kang, Y. Yang, R. K. Mahajan, J. S. Kim, H. Kim, *Biosens. Bioelectron.* **2010**, *25*, 2366.

[44] S. Park, R. S. Ruoff, *Nat. Nanotechnol.* **2009**, *4*, 217.
[45] K. Saha, S. S. Agasti, C. Kim, X. Li, *Chem. Rev.* **2012**, *112*, 2739.
[46] A. J. Bard, L. R. Faulkner, in Electrochemical Methods, Fundamentals and Applications 2nd ed.; John Wiley and Sons, New York **2001**.
[47] N. M. Markovic, T. J. Schmidt, V. Stamenkovic, P. N. Ross, *Fuel Cells* **2001**, *1*, 105.
[48] C. Song, J. Zhang, in PEM Fuel Cell Electrocatalysts and Catalyst Layers (Eds: J. Zhang), Springer, Vancouver **2008**.
[49] W. Tang, H. Lin, A. Kleiman-Shwarsctein, G. D. Stucky, E. W. McFarland, *J. Phys. Chem. C* **2008**, *112*, 10515.
[50] S. Chen, A. Kucernak, *J. Phys. Chem. B* **2004**, *108*, 3262.
[51] A. Schneider, L. Colmenares, Y. E. Seidel, Z. Jusys, B. Wickman, B. Kasemo, R. J. Behm, *Phys. Chem. Chem. Phys.* **2008**, *10*, 1931.